Eurasian J. Sci. Eng., 2023, 9(3), 47-65
https://doi.org/10.23918/eajse.v9i3p05

Published by Tishk International University
Available at: https://eajse.tiu.edu.iq/submit/

RESEARCH ARTICLE Open Access

Biosynthesis of Gold Nanoparticles with Four Different *Lactobacillus* Species

Sara Bahram Miran[1]* and Fattma Abodi Ali[2]

[1] Department of Basic Sciences, Faculty of Dentistry, Tishk International University, Erbil, Iraq
[2] Department of Medical Microbiology, College of Health Sciences, Hawler Medical University, Erbil, Iraq

Article History
Received: 17.02.2023
Revised: 13.08.2023
Accepted: 14.12.2023
Published: 02.01.2024
Communicated by: Dr. Orhan Tug
*Email address: sara.miran@tiu.edu.iq
*Corresponding Author

Abstract:

Exopolysaccharide production by many lactic acid bacteria of diverse genera and species has been widely explored. In this study, the biosynthesis of gold nanoparticles using cell-free culture supernatant of bacterial species was explored. A total of 500 saliva samples were obtained from the oral cavity, then the samples were cultured and examined. The 500 saliva samples contained 19 oral bacteria, which included *Lactobacillus fermentum*, *Lactobacillus plantarum*, *Lactobacillus casei*, and *Lactobacillus paracasei*, that extracellularly produced gold nanoparticles when exposed to chloroauric acid ($HAuCl_4$). Biosynthesis of gold nanoparticles made by reducing $HAuCl_4$ using the cell-free culture supernatant of the four different species of *Lactobacillus*. Characterizations of the gold nanoparticles were identified by Ultraviolet-Visible Spectroscopy, Fourier Transform Infrared Spectroscopy, Particle Size Analyzer (Dynamic Light Scattering), Zeta Potential, X-Ray Powder Diffraction, Transmission Electron Microscopy, Energy Dispersive X-Ray Analysis, and Atomic Force Microscopy. Given that *Lactobacillus* species are engaged in the formation of gold nanoparticles, this method may be more useful than chemical and physical methods, as it is cost-effective and eco-friendly.

Keywords: *Gold nanoparticles (AuNPs); Lactobacillus fermentum, Lactobacillus plantarum; Lactobacillus casei; Lactobacillus paracasei.*

1. Introduction

The biosynthesis of nanoparticles has attracted significant scientific attention because of their distinct and adjustable features, which have many applications in a broad spectrum of scientific and technological fields. Gold nanoparticles (AuNPs) have gained significant attention as promising candidates due to their unique physicochemical properties and possible uses in several fields such as medicine, electronics, catalysis, and imaging [1]. The conventional approaches of synthesizing AuNPs frequently include toxic chemicals and costly to-operate methods, which has led to the investigation of sustainable and ecologically friendly synthesis pathways. The utilization of biological entities to produce AuNPs has been prominent in this context. This approach exploits the natural capabilities of these entities to effectively reduce gold ions and biosynthesize nanoparticles under moderate circumstances [2].

The application of *Lactobacillus* bacteria for the biosynthesis of AuNPs has grown into a fascinating avenue for investigation within the area of nano-biotechnology. *Lactobacillus*, a genus of gram-positive bacteria, offers several advantages for the biosynthesis of AuNPs, including their abundance, safety, and ability to thrive in various environments. Biological systems, particularly microbes, provide an intriguing strategy for the synthesis of AuNPs, offering benefits in terms of environmental

sustainability and the ability to tailor nanoparticles to specific requirements. Certain strains of *Lactobacillus* species, which are well-known for their involvement in food fermentation and probiotics, have shown the capability to assist the bio reduction of gold ions into AuNPs [3]. The production of AuNPs using *Lactobacillus* bacteria is an outstanding instance of the combination of biotechnology and nanotechnology. This approach exploits the metabolic processes and biomolecules generated by these bacteria to facilitate the reduction and stability of AuNPs. The synthesis strategy used in this study is in accordance with the principles of green chemistry, since it strives to minimize the utilization of harmful reagents and energy consumption, gaining inspiration from biological processes [4].

The characterization of the synthesized AuNPs is crucial to get insights into their physicochemical properties and explore their possible uses. The distinct characteristics of AuNPs, including their dimensions, morphology, and surface composition, play a crucial role in determining their behavior and interactions within their immediate surroundings. As a result, a complete set of characterization procedures is used to thoroughly investigate these nanoparticles. The use of transmission electron microscopy (TEM) allows for the capture of high-resolution images, enabling the determination of both the size and shape of individual AuNPs [5]. Ultraviolet-visible spectroscopy (UV-Vis) enables the detection and analysis of the surface plasmon resonance (SPR) band, which is a distinctive phenomenon associated with AuNPs resulting from the collective oscillations of electrons [6]. The use of dynamic light scattering (DLS) provides valuable information on the hydrodynamic size and size distribution of AuNPs when they are suspended in a solution [7]. The use of Fourier-transform infrared spectroscopy (FTIR) is beneficial in the identification of functional groups present on the surface of nanoparticles, as well as in the elucidation of the bimolecular interactions that contribute to their stability [8].

This study focused on how gold ions are reduced to make nanoparticles in the interesting domain of AuNPs biosynthesized by four different *Lactobacillus* species using different optimizations like pH, temperature, and concentration. This research also investigates the various characterization approaches used to elucidate the structural and optical features of these biologically produced AuNPs. By putting together information from different multidisciplinary fields, our goal is to give a full picture of the opportunities and problems that come with using *Lactobacillus*-mediated AuNPs for new applications in different fields.

2. Materials and Methods

2.1 Materials

De Man, Rogosa, and Sharpe (MRS) agar and broth, chloroauric acid ($HAuCl_4.xH_2O$) (CAS Number: 27988-77-8, Sigma Aldrich®), gram stain kit (crystal violet, Gram's iodine, decolorizing agent, Safranin), hydrogen peroxide (H_2O_2), sodium hydroxide (NaOH) (CAS Number: 1310-73-2, Scharlau®), deionized distilled water (DDH_2O), ANC kit for Vitek® 2 compact system, shaker water bath, centrifuge, electronic sensitive balance, magnetic stirrer with magnetic bars, ultrasonic bath, autoclave, incubator, microbiological hood, ultraviolet–visible spectrophotometer (Thermo Scientific ™ NanoDrop ™ 2000), Fourier transform infrared spectrometer (Thermo Nicolet AVATAR 360), particle size analyzer/dynamic light scattering device (Litesizer 500), scanning electron microscope (JEOL JSM-5800LV), X-ray diffractometer (Rigaku Miniflex II), transmission electron microscope (Philips CM10), and atomic force microscope (Angstrom Advanced Inc. SPM-AA300 and Veeco Multimode Nanoscope III SPM).

2.2 Methods

2.2.1 Bacterial Isolation and Identification

A total of 500 samples of saliva were isolated from the oral cavity. The agar and broth of MRS, a selective culture medium, were prepared according to the manufacturer's instructions and sterilized by autoclaving at 121°C for 15 minutes. In a sterile environment, the samples were inoculated on MRS agar at 37°C for 24-48 hours. Then, the gram stain was stained and prepared for the catalase test; after that, a 2.7–3.3 OD600 of bacterial suspension was inoculated in Vitek® 2 compact system with the ANC kit.

2.2.2 Extracellular Biosynthesis of AuNPs Using Cell-Free Culture Supernatants (CFCS) of the Four *Lactobacillus spp.*

2.2.2.1 Preparation of Bacterial Supernatant

Aseptically, a loopful of *Lactobacillus* species bacterial isolates on MRS agar were collected and sub-cultured in MRS broth before being incubated in a shaker water bath, to increase agitation, at 37°C for 24-48 hours. The cultured broth was then centrifuged at 5000 rpm for 25 minutes at 4°C. Finally, the supernatant was collected carefully and stored at 4°C till the AuNPs were prepared.

2.2.2.2 Stock Solution Preparation for ($HAuCl_4.xH_2O$) (0.01 M)

The preparation of a stock solution of Au salts made by dissolving 0.34 g of chloroauric acid ($HAuCl_4.xH_2O$) in 100 mL of DDH_2O. The preparation of the stock concentration calculated according to the following equation:

$$\text{Molarity} = \frac{\text{Weight}}{\text{Molecular Weight}} \times \frac{1000}{\text{Volume}}$$

$$\text{Molarity} = \frac{0.34\ \text{g}}{339.79\ \text{g/mol}} \times \frac{1000\ \text{ml}}{100\ \text{ml}}$$

$$\text{Molarity} = 0.01\ \text{Molar}$$

2.2.2.3 Stock Solution Preparation for NaOH (0.4 M)

It's prepared by dissolving 4 g of Sodium hydroxide in 100 mL of DDH_2O.

$$\text{Molarity} = \frac{\text{Weight}}{\text{Molecular Weight}} \times \frac{1000}{\text{Volume}}$$

$$\text{Molarity} = \frac{16\ \text{g}}{39.997\ \text{g/mol}} \times \frac{1000\ \text{ml}}{1000\text{ml}}$$

$$\text{Molarity} = 0.4\ \text{Molar}$$

Table 1: The composition of the stock solutions used in the preparation of AuNPs

A.	Bacterial cell-free culture supernatant (CFCS)	Culture media Bacteria Incubation period Extraction method pH	: MRS broth : *Lactobacillus spp.* : 24 hours : Centrifugation at 4℃ for 25 minutes at 6000rpm : 5
B.	Stock solution of ($HAuCl_4.xH_2O$)	Molecular weight Molarity Mass Volume (DDH_2O) Mixing pH CAS number	: 339.79 g/mol : 0.01 M : 34 mg $HAuCl_4$: 100 mL : By ultrasonication for 2 min : 3 : 27988-77-8, Sigma Aldrich®
C.	Stock solution of (NaOH)	Molecular weight Molarity Mass Volume (DDH_2O) pH CAS number	: 39.997 g/mol : 0.4 M : 16 g NaOH : 1000 mL : 14 : 1310-73-2, Scharlau®

2.2.3 Biosynthesis of AuNPs by CFCS Using *L. fermentum, L. plantarum, L. casie* and *L. paracasei* Bacteria

To synthesize AuNPs, 1 mL from the prepared $HAuCl_4.xH_2O$ stock solution was diluted by 10 mL DDH_2O in 40 mL screw neck glass bottle, then 2 mL of bacterial CFCS was added drop-wise. Then the pH of this solution was adjusted to 5, 6 and 8 by adding NaOH drop-wise with a concentration of 0.4 Molar. The concentration of $HAuCl_4.xH_2O$ in this solution calculated according to the following equation:

$$(C_1 \times V_1)_{\textbf{concentrated}} = (C_2 \times V_2)_{\textbf{diluted}}.$$
$$0.01 \times 1 = C_2 \times 10$$
$$C_2 = 0.001 \text{ Molar}$$

C: concentration
V: volume
The glass tube was wrapped with aluminum foil to avoid a light reaction with AuNPs, as they turn black when exposed to light. The whole process was done while the glass tube was on the magnetic stirrer, which was left stirring for four hours. The solution became crimson after 24 hours of incubation at room temperature, indicating the existence of the AuNPs. The darkness of the red color is due to the particle size of AuNPs.

2.2.4 Characterization of Gold Nanoparticles

2.2.4.1 Ultraviolet-Visible (UV–Vis) Spectroscopy

UV-Vis spectroscopy using a spectrophotometer (Thermo Scientific ™ NanoDrop ™ 2000) at 200-700 nm confirmed nanostructure production. DDH_2O was employed as a blank solution for AuNPs in this research.

2.2.4.2 Fourier Transform Infrared Spectroscopy (FTIR) Analysis.

In order to identify the functional groups of biosynthesized AuNPs and determine the role of various reducing and capping agents in the synthesis, FTIR analysis of the AuNPs samples was performed using Thermo Nicolet AVATAR 360 spectrophotometer in the range of 4000-400 cm^{-1}.

2.2.4.3 Dynamic Light Scattering (DLS)/ Particle Size Analyzer (PSA)

The particle size analyzer (PSA) (Litesizer 500) detects particle size in liquid dispersions in the micro and millimeter range using laser diffraction.

2.2.4.4 Zeta Potential

The zeta potential was measured at 25°C to determine the stability of green synthesized AuNPs by using Litesizer 500. A volume of 25 µL of AuNPs samples were diluted 10 times with water and sonicated for 15 minutes at 20 Hz. The dilution of AuNPs were carried out to avoid the aggregation of AuNPs. Measurements were obtained in the range of -200 to +200 mV. Water was used as dispersant. Measurements were carried out in triplicates.

2.2.4.5 Energy Dispersive X-ray Spectroscopy (EDS) Analysis

A scanning electron microscope (SEM) determines a sample's chemical composition using energy dispersive X-ray spectroscopy (EDS). EDS can detect elements with atomic numbers greater than boron at 0.1% concentration. EDS may be used for material and contaminant identification, spot detection analysis up to 10 cm in diameter, quality control screening, and other applications. SEM (JEOL JSM-5800LV) was used to examine EDS to determine AuNPs form. An aluminum grid sample holder was used to dry colloidal solution drops at room temperature. EDS connected to the SEM was utilized to analyze the sample's elements.

2.2.4.6 X-ray Diffraction (XRD)

The diffraction pattern across a 2θ range of 5-120 was recorded using a Rigaku Miniflex II X-ray diffractometer (with Ni filter) and Cu Kα (k = 1.54056 Å) radiation source to determine the structure and fingerprint of crystalline metallic AuNPs. The sample container containing the AuNPs powder sample was squeezed to a smooth consistency. A thin coating of AuNPs on a tiny glass slide was measured using the same X-ray diffractometer, this time with Ni-filtered Cu Kα radiation (λ = 0.15406 nm). The resulting diffractogram was then compared to the international center for diffraction data (ICDD) standard database. The diffraction intensities were tested from a 2θ angle of 30° to 80°.

2.2.4.7 Transmission Electron Microscopy (TEM)

The AuNPs solution was sonicated for 15 minutes to eliminate possible aggregates. A tiny amount of this sonicated solution was placed on a carbon-coated copper grid and dried under infrared light to evaporate the solvent. High-quality TEM images were taken using a Philips CM10 TEM at 200 kV with 0.23 nm resolution. Histograms showed the AuNPs size distribution from Image J program.

2.2.4.8 Atomic Force Microscopy (AFM) Analysis

Atomic Force Microscopy was used to assess the topographical morphology, size, and surface features of AuNPs on cleaned 20 mm^2 × 20 mm^2 mica sheets glued to metal pads. The dissolved liquid washed the AuNPs off the mica sheet three to four times after 5 minutes at room temperature. The AuNPs

solution was dispersed on a freshly cut mica (Grade II) substrate to make AFM samples. Nitrogen dried the solvent. AFM was performed in intermittent contact mode using a Veeco Multimode Nanoscope III Scanning Probe Microscope (SPM). Arrow-NCR etched Si AFM tips resonated at 300 kHz. Angstrom Advanced Inc. SPM-AA300 can photograph AuNPs' topography and surface at high resolution. Five drops of AuNPs were applied to cover slide in oven at 110 °C for 30 minutes. The probe-sample response may reveal the sample's surface and three-dimensional topography. AFM probes have a sharp tip and a tiny cantilever that detects probe-sample contact. Many forces affect the probe-sample surface contact. Cantilever bending, following Hook's law, measures the probe-sample normal force.

$$F = k \Delta z$$

Where: k is the spring constant of the cantilever, Δz is the cantilever bending in nm.

3. Findings and Discussion

3.1 Identification of *Lactobacillus spp.*

Isolation of *Lactobacillus spp.* was obtained by using a selective enrichment culture technique that is culturing the cell on MRS agar which allows selectively growth of *Lactobacillus spp.* and prevents other species. Macroscopically, the isolates were identified as related to the genus *Lactobacillus spp.* whose texture outcome on MRS agar was white, greyish white or cream in color, with size varying from 0.5 to 2.3 mm in diameter, with entire or undulate margins, convex, smooth, glistening colonies, and opaque without pigment on MRS agar. Microscopically, the bacteria appeared under oil immersion using a lens (100x) as gram-positive, bacilli, arranged singly, in pairs, or in short chains as shown in Figure (1). After the growth of the isolates on MRS agar yielded a positive gram stain and a negative catalase test, they were exposed to the Vitek® 2 Compact system using the ANC kit.

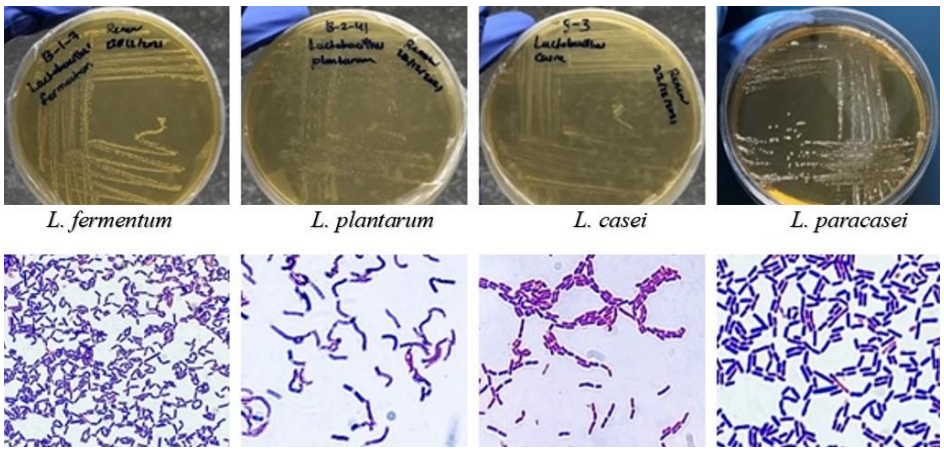

Figure 1: Macroscopic, microscopic and morphologic examination of the four different species of *Lactobacillus* bacterial isolates on MRS agar plates.

3.2 Preparation of Bacterial Cell-Free Culture Supernatant (CFCS)

The results demonstrated that after inoculating MRS broth with a 24-hour culture of *Lactobacillus spp.* on MRS agar, 24-hour incubation in a shaker water bath resulted in a higher growth rate than 24-hour incubation in a conventional incubator. The results also showed that using a cold 4ºC centrifuge gave a better result for separating the extracellular components from the bacteria since it would protect the extracellular components from degrading by centrifugation. The CFCS of *L. fermentum*, *L. plantarum*,

L. casei, and *L. paracasei* were yellow in color, the stock solution of $HAuCl_4$ was golden yellow in color, and the stock solution of NaOH was also colorless and transparent, as featured in Figure (2).

Figure 2: The stock solutions used in the preparation of AuNPs. (A) *Lactobacillus* CFCS, (B) stock solution of ($HAuCl_4.xH_2O$), and (C) stock solution of (NaOH).

3.3 The Optimization of AuNPs Biosynthesis

Extracellular biosynthesis of AuNPs by the CFCS of *Lactobacillus spp. (L. fermentum, L. plantarum, L. casei, and L. paracasei)* with $HAuCl_4$, 1 mM was investigated. The results showed that no color change was observed upon the onset of AuNPs preparation. After 24 hours of incubation at room temperature (25℃), the color of the solution turned pink. Then, after storing the solution for 72 hours at room temperature, the color of the solution turned red wine in color. As a result, color change was detected in the preparation of AuNPs based on time optimization. The picture of test tubes of $HAuCl_4$ solution after exposure to CFCS of *Lactobacillus spp.* is shown in the inset of Figure (3). Based on temperature optimization, the room temperature (25℃) and the body temperature (37℃) were used and both produced AuNPs. The temperature was adjusted by incubating the samples inside an incubator.

Optimization of AuNPs utilizing different ratios of CFCS to $HAuCl_4$ After incubation, the ratio of CFCS to $HAuCl_4$ was the best at 1:10, respectively, as illustrated in Figure (4). The darker the color the larger the particle size of the AuNPs. In the preparation of AuNPs, based on the pH optimization, three different pH were used (pH 5, 6, and 8), as shown in Figure (5). The finding showed that stirring for two hours, incubation time 24 to 72 hours, and pH 5,6, and 8 had an impact on AuNPs biosynthesis and the best optimization for time was 24 hours after incubation, for pH was 8, and for concentration was a ratio 1:10.

Figure 3: (A) The onset of AuNPs preparation, (B) AuNPs preparation after 24 hours, and (C) AuNPs preparation after 72 hours

Figure 4: AuNPs at different concentrations. (A) 1:10, and (B) 1:5, cell-free-supernatant: $HAuCl_4$, respectively

Figure 5: AuNPs at different pH. (A) AuNP at pH 5, (B) AuNP at pH 8, (C) AuNP at pH 6.

3.4 Characterization of AuNPs

3.4.1 Optical Properties of AuNPs (UV-Visible Spectroscopy)

The results confirm that the surface plasmonic resonance appears in all the prepared AuNPs samples with an absorption peak ranging between (531–545) nm, as shown in Figure (6).

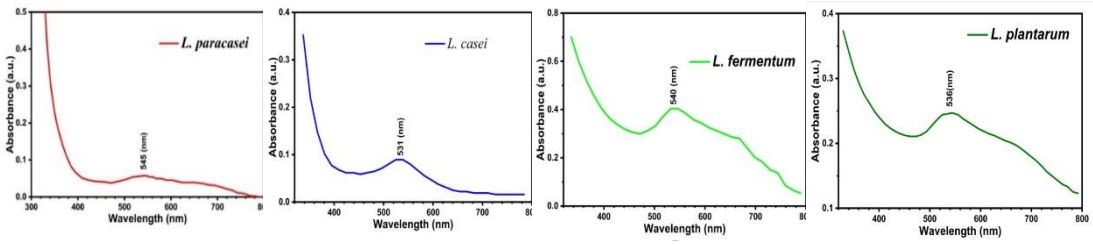

Figure 6: UV–visible absorption spectrum of AuNPs by *L. paracasei* (545 nm), *L. casei* (531 nm), *L. fermentum* (540 nm), and *L. plantarum* (536 nm).

3.4.2 Fourier Transform Infrared Spectroscopy (FTIR) of AuNPs

All results of the FTIR spectrum of AuNPs biosynthesized by *L. paracasei. L. casei*, *L. fermentum*, and *L. plantarum* had four peaks, indicating the emergence of vibrations and absorptions for functional groups. The primary peak values exhibited medium-sharp O-H stretching vibrations in the hydroxyl group (alcohol) at FTIR spectra of 3724 cm^{-1}, 3713 cm^{-1}, 3756 cm^{-1}, and 3781 cm^{-1}, respectively. The secondary peak values exhibited peak values for strong O=C=O stretching vibrations in the alkene group (carbon dioxide) at 2352 cm^{-1}, 2348 cm^{-1}, 2381 cm^{-1}, and 2338 cm^{-1}, respectively. The third peak values exhibited strong P-OR stretching vibrations in the ester group at 903 cm^{-1}, 903 cm^{-1}, 904 cm^{-1}, and 900 cm^{-1}, respectively. The fourth and last peak values exhibited strong C-I bending vibrations at 450 cm^{-1}, 477 cm^{-1}, 459 cm^{-1}, and 491 cm^{-1}, respectively, as shown in Figure (7).

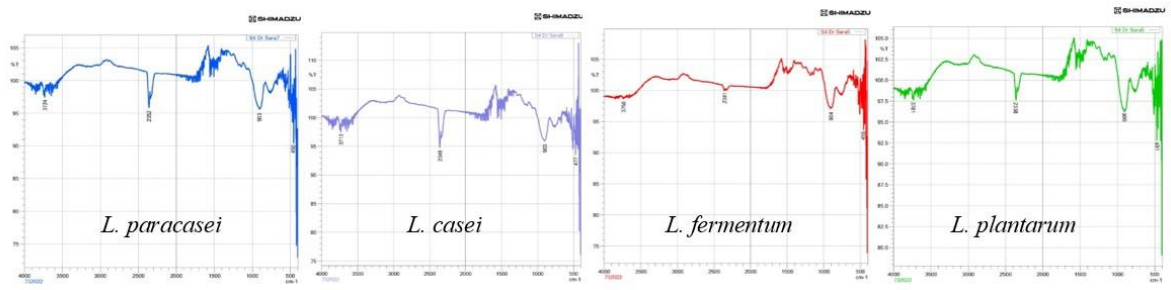

Figure 7: FTIR distribution of AuNPs by *L. paracasei. L. casei*, *L. fermentum*, and *L. plantarum*.

3.4.3 Particle Size and Distribution of AuNPs (DLS)

Dynamic Light Scattering measurement of the particle size and distribution of AuNPs indicated the hydrodynamic diameter and polydispersity index. The results of particle size distribution of AuNPs biosynthesized by *L. paracasei* confirmed that the hydrodynamic diameter was 65.30 nm and the polydispersity index was 25.4 %. A low polydispersity value indicates a good particle distribution in the solution. As for the AuNPs biosynthesized by *L. casei*, the results indicate that the hydrodynamic diameter was 68.20 nm and the polydispersity index was 22.7 %, with a perfect particle distribution. The hydrodynamic diameter of the AuNPs biosynthesized by *L. fermentum* grew to 127.29 nm with a polydispersity index of 27%. While the hydrodynamic diameter of the AuNPs biosynthesized by *L.*

plantarum was 139.67 nm, with a polydispersity index of 25.3%. These results confirm that the particle scattering is good with no wide particle distribution in the solution, as shown in Figure (8).

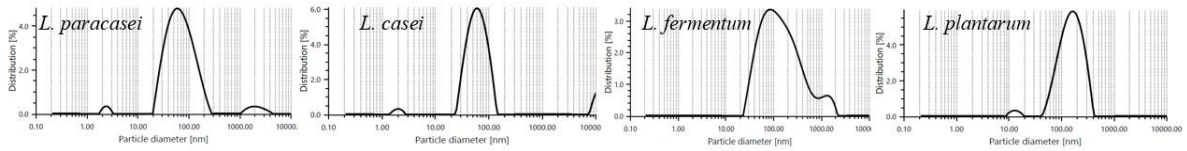

Figure 8: DLS of the AuNPs biosynthesized by *L. paracasei. L. casei*, *L. fermentum*, and *L. plantarum*.

In comparing between samples, the AuNPs by *L. paracasei* have the smallest hydrodynamic diameter, followed by the AuNPs formed from *L. casei* with a slight difference in diameter, while the AuNPs by *L. plantarum* and *L. fermentum* have significantly increased in hydrodynamic diameter compared with AuNPs by *L. paracasei* and *L. casei*. All samples show a polydispersity index of less than 30%, which confirms the high dispersion and good particle distribution in aqueous solutions, see Figure (9).

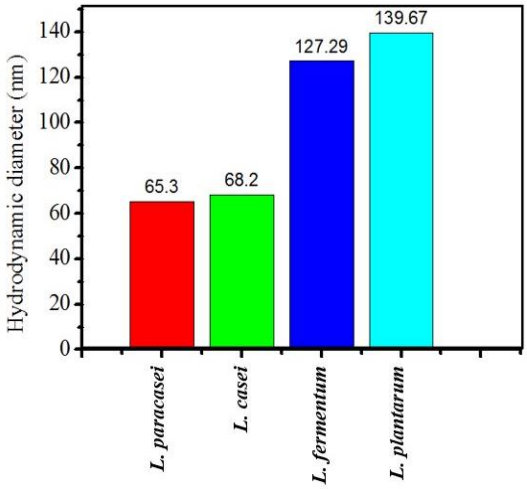

Figure 9: DLS for each sample of AuNPs.

3.4.4 Zeta Potential of AuNPs

The zeta potential distribution of AuNPs biosynthesized by *L. paracasei*, according to the results, the average zeta potential of the suspensions is -21.7 mV, suggesting that they are incipiently stable. Concerning the AuNPs produced by *L. casei*, the data show that the mean zeta potential is -29.5 mV, indicating that the suspensions are moderately stable. While the AuNPs biosynthesized by *L. fermentum*, the results are depicted that the mean zeta potential is -19.1 mV, and colloid suspensions are incipiently stable. Regarding the zeta potential distribution of AuNPs biosynthesized by *L. plantarum*, the results show that the mean zeta potential of colloid suspensions is -28.0 mV and that they are moderately stable, see Figure (10).

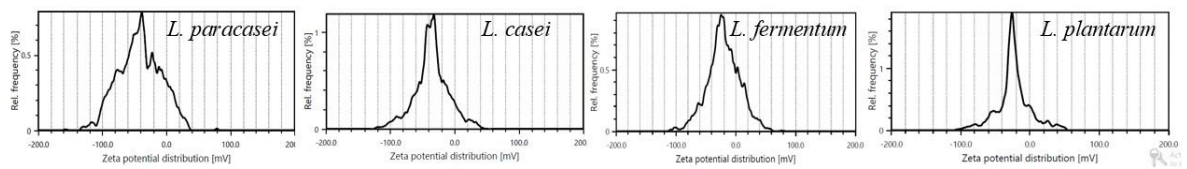

Figure 10: Zeta potential distribution of the AuNPs biosynthesized by *L. paracasei. L. casei*, *L. fermentum*, and *L. plantarum*.

When comparing between the samples, the findings confirmed that *L. casei* had the greatest zeta potential and *L. fermentum* had the lowest, as indicated in Figure (11). This suggests that AuNPs produced by *L. casei* and *L. plantarum* are more stable during colloidal dispersion in aqueous solutions, resulting in reduced agglomeration and loss of surface characteristics at the nanoscale.

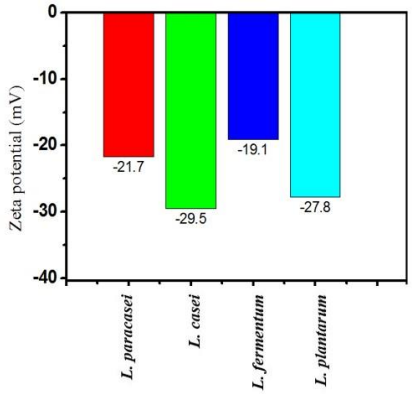

Figure 11: Zeta potential of AuNPs biosynthesized from different *Lactobacillus spp.* by (Litesizer).

3.4.5 X-ray Diffraction (XRD)

The X-ray diffraction pattern for biosynthesized AuNPs is shown in Figure (12). The microorganisms *L. paracasei*, *L. casei*, *L. fermentum*, and *L. plantarum*, denoted by L.Pa, L.C, L.Fe, and L.Pl, respectively. It serves as a reducing agent for $HAuCl_4$ and varies in the degree to which it can reduce; accordingly, the behavior of the XRD pattern for Au-L.C may be considered the best ability to reduce, according to the clear diffraction peaks for AuNPs with some impurities like peaks for NaCl. There are four diffraction angles with different intensities depend on types of bacteria and this peaks conforming the cubic structure of AuNPs according to 38.2º, 44.3º, 64.8º, 77.5º. Corresponding to (111), (200), (220), and (311), respectively as shown in Table (2).

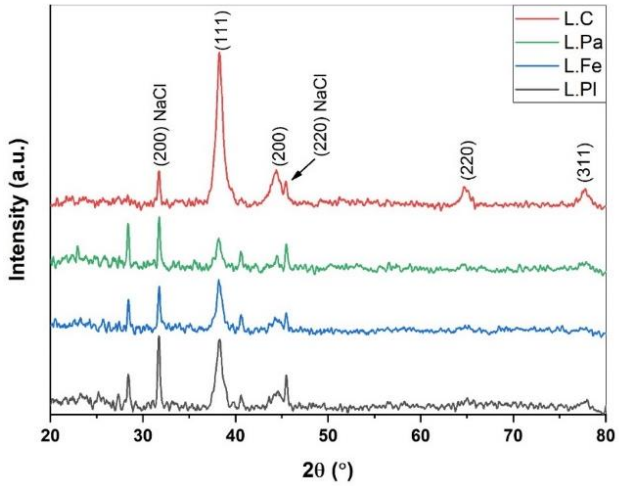

Figure 12: XRD pattern for AuNPs prepared by biosynthesis method

In perspective of AuNPs crystallite size, the lowest crystallite size for AuNPs - *L.paracasei* is 17.3 nm, while the largest crystallite size for AuNPs-*L. plantarum* is 29nm, the details presented in Figure (13).

Table 2: Crystallite size for AuNPs prepared by biosynthesis for four different *Lactobacillus spp.*

Samples	2 theta (degree)	hkl (panel)	FWHM (deg)	2 theta (Rad.)	FWHM (Rad.)	D (nm)
AuNPs-*L. casei*	38.2427	(111)	0.3936	0.230	0.007	20.721
	44.3067	(200)	0.7872	0.310	0.014	10.593
	64.8626	(220)	0.96	0.566	0.017	9.801
	77.5404	(311)	0.1718	0.677	0.003	59.286
AuNPs-*L. paracasei*	38.2485	(111)	0.6298	0.230	0.011	12.950
	45.5085	(200)	0.384	0.310	0.007	21.715
AuNPs-*L. fermentum*	38.2984	(111)	0.6298	0.230	0.011	12.950
	44.8506	(200)	0.2426	0.310	0.004	34.372
AuNPs-*L. plantarum*	38.2381	(111)	0.9446	0.230	0.016	8.634
	44.8581	(200)	0.3633	0.310	0.006	22.953
	77.5304	(220)	0.1855	0.677	0.003	54.904

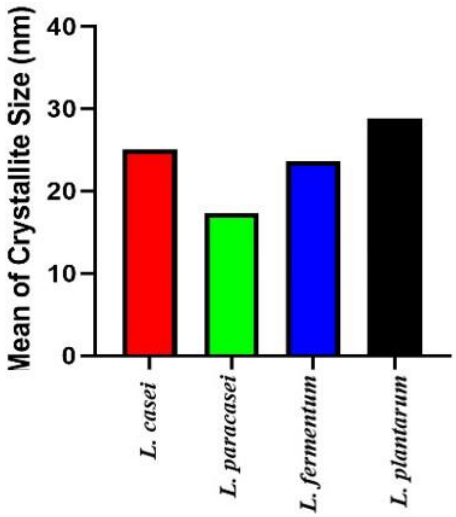

Figure 13: Mean of crystallite size for AuNPs prepared by biosynthesized by different *Lactobacillus spp.*

3.4.6 Energy Dispersive X-ray Spectroscopy (EDS) of AuNPs

The elemental composition of the AuNPs and their surroundings were examined using the EDS measurements. The results of EDS for the AuNPs made by *L. paracasei* observed that the AuNPs had (4.3%) of the weight of O, and (95.7%) of the weight of Au. The discoveries revealed the presence of metallic Au. There was a trace of O and a significant amount of Au. The results of EDS for the AuNPs made by *L. casei* proved that the AuNPs had (34.2%) of the weight of O, and (65.8%) of the weight of Au. The findings of EDS for the AuNPs made by *L. fermentum* indicated that the AuNPs had (45.6%) of the weight of O, and (54.4%) of the weight of Au. The outcomes of EDS for the AuNPs made by *L. fermentum* demonstrated that the AuNPs had (33.6%) of the weight of O, and (66.4%) of the weight of Au. The EDS spectrum of the AuNPs biosynthesized by *Lactobacillus spp.* indicated strong signal peaks at 2.15 keV, which corresponds to elemental Au. The EDS detector also gave the peaks of sodium at 1.041 keV and chloride 2.621 keV indicating impurities in the AuNPs samples, as illustrated in Figure (14).

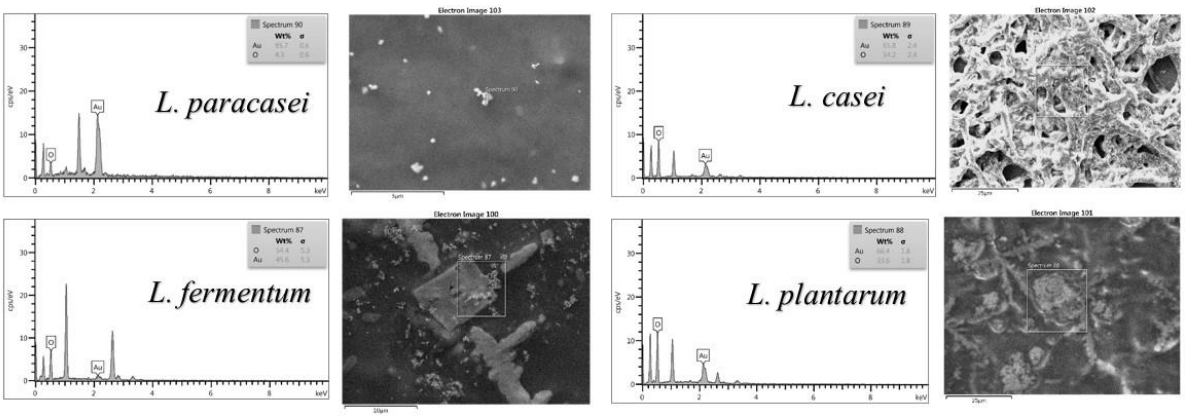

Figure 14: EDS spectra of the AuNPs biosynthesized by *L. paracasei. L. casei, L. fermentum,* and *L. plantarum*.

3.4.7 Transmission Electron Microscopy (TEM) of AuNPs

Analysis of the AuNPs biosynthesized by the *L. paracasei* using TEM reveals significant particle aggregation, which increases the size. This behavior may be related to the kind of bacteria that are involved in this aggregate and play a significant role. The histogram size distribution explains to us the greater particle size between 80 and 100 nm and the average particle size of around 76.7 nm.

Examination of the shape and particle size of AuNPs biosynthesized by *L. casei,* the TEM pictures at various magnifications showed the AuNPs along with adhesion nanoparticles with each other. As a result, the size distribution of particle size of around 29 nm can be observed. This form may be due to the behavior of the bacterial strain utilized throughout the preparation processes.

According to TEM observations, AuNPs biosynthesized by employing *L. fermentum* bacteria as a reducing agent have a distinctive shape and are practically semi-spherical, with an average particle size of around 25.44 nm. Some of the particles are depicted as hexagonal shapes, verifying the sample's structure. The size distribution histogram illustrates the density of the size distribution between 20 and 30 nm.

The TEM images of biosynthesized AuNPs by *L. plantarum* reveal that the average particle size of AuNPs is about 27.6 nm. This size range helps AuNPs be more useful in biological uses. Additionally, the efficiency of the smaller particle size has increased due to its increased capacity to penetrate bacterial cell walls, see in Figure (15).

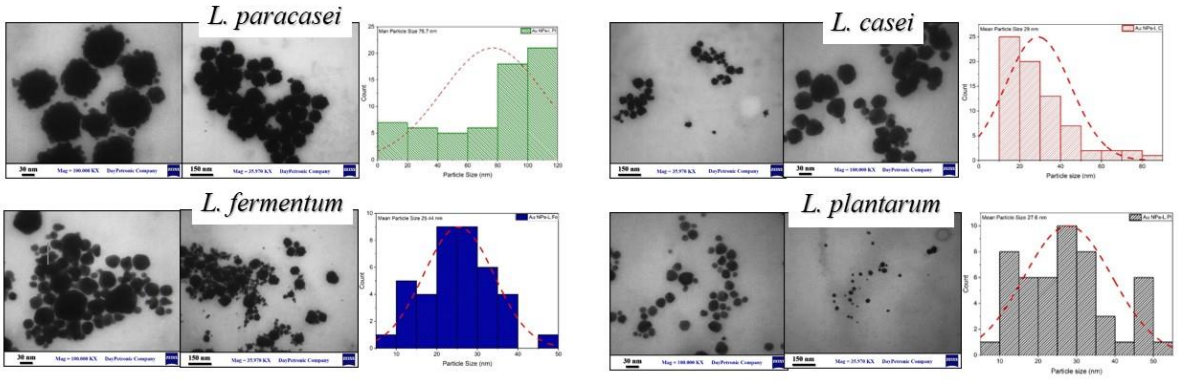

Figure 15: TEM Image of AuNPs with histogram particle size biosynthesized by *L. paracasei*. *L. casei*, *L. fermentum*, and *L. plantarum*.

3.4.8 Atomic Force Microscopy (AFM) of AuNPs

Atomic force microscopy is a potent imaging method that enables the structural characterization of individual molecules with nanoscale resolution. The results of AFM analysis of the surface topography with the histogram of particle analysis of the AuNPs biosynthesis using *L. paracasei*, indicated that the initial impression confirms the presence of agglomerations of particles of different sizes. The 3D roughness average (Sa) was 19.28 nm and the root mean square roughness (Sq) was 29.51 nm. While the AFM analysis of AuNPs biosynthesis using *L. casei* indicated an increase in particle aggregation with (Sa) of 179.6 nm and (Sq) of 214.6 nm. Concerning the AFM for AuNPs biosynthesis using *L. fermentum*, *the* findings confirmed that the surface topography shows a change in shape with a decrease in the height of the nano-plateaus with (Sa) of 3.6 nm and (Sq) of 5.2 nm. Furthermore, the AFM for AuNPs biosynthesis using *L. plantarum*, the outcomes indicated the presence of spherical AuNPs with a variation in the height of the surface topography, with (Sa) of 31.65 nm and (Sq) of 52.69 nm, as illustrated in Figure (16).

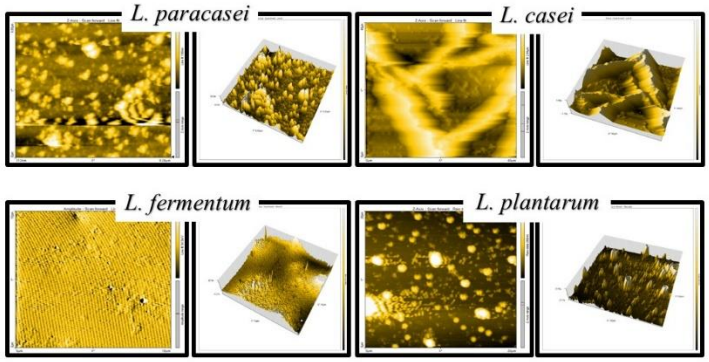

Figure 16: Two and Three - dimensional (2D-3D) AFM topography images of AuNPs biosynthesized by *L. paracasei*. *L. casei*, *L. fermentum*, and *L. plantarum*.

A comparison of the histogram results for the average roughness values for all biosynthesized AuNPs samples by AFM showed that the highest surface roughness of AuNPs was by *L. casei* and the least surface roughness of AuNPs was by *L. fermentum*, as illustrated in Figure (17).

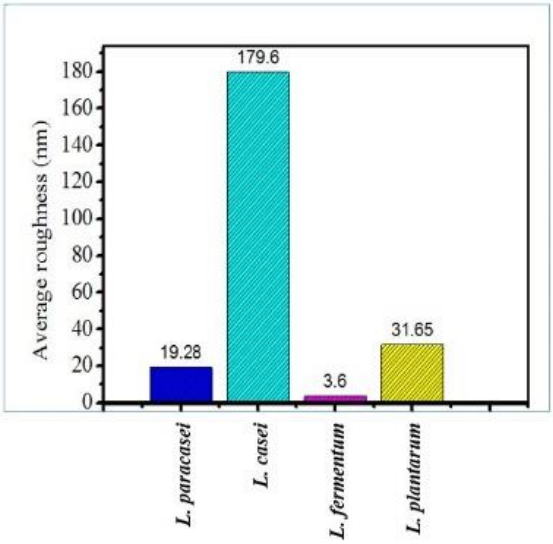

Figure 17: Displays a histogram of the average roughness values for all biosynthesized AuNPs samples by AFM.

4. Discussion

The extracellular synthesis of AuNPs utilizing CFCS of *Lactobacillus spp*. is evident from the pink-to-wine-red color seen in the reaction mixture. The pink-to-wine-red hue of the colloidal gold solution is caused by the activation of surface plasmon vibrations in nanoparticles and serves as a simple spectroscopic marker of their production [9].

Several hydroquinones with outstanding redox characteristics that potentially operate as electron shuttles in metal reductions have been identified [10, 11]. As a result, it was clear that the electron shuttle or other reducing agents produced by *Lactobacillus spp.* are capable of reducing gold ions to AuNPs. In the absence of CFCS, however, gold ion reduction did not occur. This clearly shows that the reducing agents produced in the cultures of the previously indicated *Lactobacillus spp.* are engaged in the reduction process. Thus, electron shuttles or other reducing agents produced by *Lactobacillus spp.* are clearly capable of reducing gold ions to AuNPs.

When examining the characteristics of nanoparticles, research on the optical properties of nanoparticles is critical. The electromagnetic radiation absorption spectrum is a key aspect in studying surface plasmon resonance, which is a property of metallic nanoparticles, such as AuNPs [12, 13]. The spectra of *L. paracasei* match the conventional spectrum of AuNPs [14].

The surface plasmonic resonance absorption peak was 545 nm after employing *L. paracasei* bacteria, while the lowest absorption peak was 531 nm after utilizing *L. casei* bacteria. This property, which can be observed on the surfaces of different metal nanoparticles such as AuNPs, is caused by free electrons in the nanoparticles migrating together when light hits them. The blue shift and red shift may explain the difference in the peak surface plasmonic resonance peak of nanoparticles. The blue shift (short wavelengths) signifies a reduction in nano sizes caused by quantum confinement, while the redshifts (long wavelengths) show an increase in nano sizes [15,16,17].

In this study, the FTIR analysis was used to characterize the chemical surface of the AuNPs biosynthesized using the CFCS of *L. fermentum, L. plantarum, L. casei, and L. paracasei*. All results of FTIR in the study showed that the AuNPs from all *Lactobacillus spp*. made four peaks. The primary

peaks were ranging from 3713-3758 cm^{-1} that may be attributed to the (O-H) stretching groups of polysaccharide. This result was in accordance with a previous study that demonstrated the presence of a broadly stretching intense peak at around 3428 cm^{-1} which is characteristic of hydroxyl groups (O-H) and (C-H) model between 2854 and 2925 cm^{-1} [18]. The secondary peaks were ranging from 2381-2338 cm^{-1} that may be attributed to the O=C=O stretching groups of carbon dioxide. The tertiary peaks were ranging from 904-900 cm^{-1} that may be attributed to the C=C bending groups of alkane. The quaternary peaks were ranging from 450-491 cm^{-1} that may be attributed to the C-I stretching groups of halo compound which may be due to the impurities from NaCl. A previous study showed that the band at 491 cm^{-1} may be ascribed to Mg–O–In chains in the In-HT structure and the bands at 446 and 450 cm^{-1} to the In–O–In linkages [19].

Dynamic light scattering is used to measure the diameter and distribution of nanoparticles distributed in liquid [20]. It is also used to calculate the polydispersity index, which ranges from 0.0 (for a completely uniform particle size sample) to 1.0 (for a highly polydisperse sample with various particle size populations) [21]. International Organization for Standardization (ISO) has determined that polydispersity values larger than 0.7 are frequent in a wide size variety of particles, but values less than 0.05 are more prevalent in monodisperse samples [22]. This study's findings demonstrate that particle scattering is excellent, with no large particle dispersion in the solution. When comparing, *L. paracasei* has the shortest hydrodynamic diameter, followed by *L. casei*, which has a slightly larger diameter. While *L. fermentum* and *L. plantarum* have a much larger hydrodynamic diameter than *L. paracasei* and *L. casei*. The polydispersity index for all samples is less than 30%, confirming the high dispersion and excellent particle distribution in aqueous solutions.

The particle's zeta potential is one of the most critical properties that may influence both cell adhesion and stability. The (negative or positive) zeta potential values have a considerable impact on particle suspension stability. This is due to particle segregation generated by electrostatic repulsion between particles of the same electric charge [23]. Table (3) describes the stability at each zeta-potential range [24] .

Table 3: Colloidal stability of zeta potential.

Zeta potential (mV)	Colloid stability
0 to ±5	Rapid agglomeration
±10 to ±30	Incipient stability
±30 to ±40	Moderate stability
±40 to ±60	Good stability
Above ±60	Excellent stability

The *L. paracasei* findings suggested that the suspensions are incipiently stable, similarly to a previous study [25]. When the zeta potential of the samples was compared, the findings revealed that *L. casei* had the greatest value and *L. fermentum* had the lowest. This suggests that AuNPs produced by *L. casei* and *L. plantarum* are more stable during colloidal dispersion in aqueous solutions, resulting in reduced agglomeration and loss of surface characteristics at the nanoscale.

The X-ray diffraction is an important technique for determining crystal structure; it determines atomic arrangement, lattice parameters, and crystalline size [26]. The XRD pattern of AuNPs is generated by a biosynthetic process using *L. casei, L. paracasei, L. fermentum,* and *L. plantarum* bacteria. The CFCS of them functions as a reducing agent for $HAuCl_4$, and their capacity to reduce varies; as a result, the

behavior of the XRD pattern for AuNPs by *L. casei* may be deemed to have the greatest ability to reduce, based on clearly diffraction peaks for AuNPs with certain impurities, such as peaks for NaCl.

This diffraction angle corresponds to JCPDS Card No: (002-1095) Debye Scherrer's formula was used to compute the crystallite size of AuNPs [26]:

$$\text{Crystallite size(D)} = \frac{0.9\lambda}{\beta cos\theta}$$

Where D denotes the crystal size, and = 1.5406 A^{o} is the X-ray wavelength, is the peak's full-width half maximum (FWHM) in radians, and is the Bragg angle. *L. paracasei* synthesized the lowest crystallite size AuNPs, while *L. plantarum* synthesized the largest crystallite size for AuNPs. All the measurements showed that the aqueous bacterial extracts of *L. paracasei, L. casei, L. fermentum,* and *L. plantarum* could be used to effectively produce AuNPs. The EDS study revealed that *L. paracasei* formed the particles completely of elemental gold, identical to what was discovered by Gannimani et al. in 2014 [27].

The shape of AuNPs might be attributed to the bacterial strain utilized in the preparation operations. The biosynthesis of AuNPs using the *L. paracasei* strain indicated a lot of particle aggregation, which leads to an increase in size; this behavior may be bacterial-like and play a crucial role in this aggregate. The aggregation led to the complete loss of biological activity, and this aggregation returns to numerous causes, but the three most probable are pH, the influence of NaCl, and the effect of glucose and glutamine [28]. Furthermore, the difference in large aggregation has a bigger impact on nanoparticle stability, which may be assessed using zeta potential [29]. The biosynthesis of AuNPs by *L. plantarum* produced spherical AuNPs without aggregations with an average particle size of about 27.6 nm, and this size range resulted in more active nanoparticles in biological applications. Additionally, the small particle size has more ability to penetrate the bacterial wall membrane, making it more effective, similar to previous studies [30]. The findings show that the greatest average roughness was obtained after using *L. casei* bacteria and the lowest average roughness was obtained after using *L. fermentum*. The increase in roughness may be due to the action of *L. casei* bacteria, which causes variation in nano shapes and sizes, resulting in an increase in contact sites on the nanoparticle surface.

5. Conclusion

The AuNPs have been synthesized by the reduction of Au^{3} to Au^{0} by using a CFCS of *L. paracasei, L. casei, L. fermentum,* and *L. plantarum*. The function of CFCS is twofold: first, to act as a reducing agent, and second, as a capping agent. The concentration ratio of CFCS to [Au^{3}] can be used to adjust the mean diameter of AuNPs (1-100 nm). The pH of the solution can be used to regulate the shape of AuNPs (1-100 nm). The pH of the solution is necessary to be adjusted alkaline. Centrifugation and filtration by filter paper are enough for the purification of CFCS. The ratio of CFCS to $HAuCl_4$ is necessarily adjusted to 1:10 for AuNPs synthesis, the more the reducing agent the larger the particle size. The storage of the AuNPs is necessary to be kept at 4 °C to avoid aggregation of the particles and wrapped with aluminum foil to prevent light reactions.

It is recommended to further research the purification processes of AuNPs and determine the biological agents that can work as reducing and capping agents. In conclusion, the biosynthesis of AuNPs by *Lactobacillus* species is a promising area of research. *Lactobacillus* species can create AuNPs by reducing gold ions. This eco-friendly method has easy reaction conditions and several applications. The reaction parameters may regulate AuNPs size, shape, and stability. The biosynthesis of AuNPs by

Lactobacillus species has significant promise for sustainable and biocompatible AuNPs synthesis, but further study is required to understand the processes and improve the synthesis process.

6. Author's Contribution

We confirm that the manuscript has been read and approved by all named authors. We also confirm that each author has the same contribution to the paper. We further confirm that the order of authors listed in the manuscript has been approved by all authors.

7. Conflict of interest

There is no conflict of interest for this paper.

8. Acknowledgment

I would like to express my genuine thanks and high appreciation to Asst. Prof. Laith Ahmad Yaaqoob from the College of Science/Baghdad University, Dr. Ary Agha from Rizgari Teaching Hospital, and Asst. Prof. Rebwar Hamasalih from the College of Education at Salahaddin University, whose support, genuineness, and guidance efforts made my work much easier.

References

[1] Dreaden EC, Alkilany AM, Huang X, Murphy CJ, El-Sayed MA. The golden age: gold nanoparticles for biomedicine. Chemical Society Reviews. 2012; 41(7): 2740-79. https://doi.org/10.1039/C1CS15237H.

[2] Iravani S. Green synthesis of metal nanoparticles using plants. Green Chemistry. 2011; 13(10): 2638-50. https://doi.org/10.1039/C1GC15386B.

[3] Hussain I, Singh NB, Singh A, Singh H, Singh SC. Green synthesis of nanoparticles and its potential application. Biotechnology letters. 2016 Apr; 38: 545-60. https://doi.org/10.1007/s10529-015-2026-7.

[4] Ahmed S, Ikram S. Biosynthesis of gold nanoparticles: a green approach. Journal of Photochemistry and Photobiology B: Biology. 2016 Aug 1; 161: 141-53. https://doi.org/10.1016/j.jphotobiol.2016.04.034.

[5] Titus D, Samuel EJ, Roopan SM. Nanoparticle characterization techniques. InGreen synthesis, characterization and applications of nanoparticles 2019 Jan 1 (pp. 303-319). Elsevier. https://doi.org/10.1016/B978-0-08-102579-6.00012-5.

[6] Saha K, Agasti SS, Kim C, Li X, Rotello VM. Gold nanoparticles in chemical and biological sensing. Chemical reviews. 2012 May 9; 112(5): 2739-79. https://doi.org/10.1021/cr2001178.

[7] Bhattacharya D, Gupta RK. Nanotechnology and potential of microorganisms. Critical reviews in biotechnology. 2005 Jan 1; 25(4): 199-204. https://doi.org/10.1080/07388550500361994.

[8] Dwivedi AD, Gopal K. Biosynthesis of silver and gold nanoparticles using Chenopodium album leaf extract. Colloids and Surfaces A: Physicochemical and Engineering Aspects. 2010 Oct 20; 369(1-3): 27-33. https://doi.org/10.1016/j.colsurfa.2010.07.020.

[9] Ashajyothi, Chandrakanth RK. Biological Synthesis and Characterization of Gold Nanoparticles from Enterococcus faecalis. Journal of bionanoscience 2014 Aug 01; 8(4): 255-259. https://doi.org/10.1166/jbns.2014.1232.

[10] Rajeshkumar S. Anticancer activity of eco-friendly gold nanoparticles against lung and liver cancer cells. Journal of Genetic Engineering and Biotechnology 2016 Jun; 14(1): 195-202. https://doi.org/10.1016/j.jgeb.2016.05.007.

[11] Thakker JN, Dalwadi P, Dhandhukia PC. Biosynthesis of Gold Nanoparticles Using Fusarium oxysporum f. sp. cubense JT1, a Plant Pathogenic Fungus. ISRN Biotechnology 2013; 2013: 515091-5. http://dx.doi.org/10.5402/2013/515091.

[12] Sosa IO, Noguez C, Barrera RG. Optical Properties of Metal Nanoparticles with Arbitrary Shapes. The journal of physical chemistry. B 2003 Jul 03,; 107(26): 6269-6275. https://doi.org/10.1021/jp0274076.

[13] Amendola V, Pilot R, Frasconi M, Maragò OM, Iatì MA. Surface plasmon resonance in gold nanoparticles: a review. Journal of Physics: Condensed Matter. 2017 Apr 20; 29(20): 203002. https://doi.org/10.1088/1361-648x/aa60f3.

[14] Ngo VKT, Nguyen HPU, Huynh TP, Tran NNP, Lam QV, Huynh TD. Preparation of gold nanoparticles by microwave heating and application of spectroscopy to study conjugate of gold nanoparticles with antibody E. coli O157:H7. Adv Nat Sci: Nanosci Nanotechnol 2015 -07-02; 6(3). http://dx.doi.org/10.1088/2043-6262/6/3/035015.

[15] Meva FE, Segnou ML, Ebongue CO, Ntoumba AA, Kedi PB, Deli V, Etoh MA, Mpondo EM. Spectroscopic synthetic optimizations monitoring of silver nanoparticles formation from Megaphrynium macrostachyum leaf extract. Revista Brasileira de Farmacognosia. 2016 Oct; 26: 640-6. https://doi.org/10.1016/j.bjp.2016.06.002.

[16] Niu J, Shin YJ, Son J, Lee Y, Ahn JH, Yang H. Shifting of surface plasmon resonance due to electromagnetic coupling between graphene and Au nanoparticles. Optics express. 2012 Aug 27; 20(18): 19690-6. https://doi.org/10.1364/OE.20.019690.

[17] Ren Y, Qi H, Chen Q, Wang S, Ruan L. Localized surface plasmon resonance of nanotriangle dimers at different relative positions. Journal of Quantitative Spectroscopy and Radiative Transfer. 2017 Sep 1; 199: 45-51. https://doi.org/10.1016/j.jqsrt.2017.05.003.

[18] Singh RP, Shukla MK, Mishra A, Kumari P, Reddy CR, Jha B. Isolation and characterization of exopolysaccharides from seaweed associated bacteria Bacillus licheniformis. Carbohydrate polymers. 2011 Mar 17; 84(3): 1019-26. https://doi.org/10.1016/j.carbpol.2010.12.061.

[19] Frost RL, Palmer SJ, Grand LM. Synthesis and Raman spectroscopy of indium-based hydrotalcites of formula Mg6In2 (CO3)(OH) 16· 4H2O. Journal of Raman Spectroscopy. 2010 Dec; 41(12): 1797-802. https://doi.org/10.1002/jrs.2571.

[20] Adebayo-Tayo B, Salaam A, Ajibade A. Green synthesis of silver nanoparticle using Oscillatoria sp. extract, its antibacterial, antibiofilm potential and cytotoxicity activity. Heliyon. 2019 Oct 1; 5(10). https://doi.org/10.1016/j.heliyon.2019.e02502.

[21] Danaei M, Dehghankhold M, Ataei S, Hasanzadeh Davarani F, Javanmard R, Dokhani A, et al. Impact of Particle Size and Polydispersity Index on the Clinical Applications of Lipidic Nanocarrier Systems. Pharmaceutics 2018 May 18,; 10(2): 57. https://doi.org/10.3390/pharmaceutics10020057.

[22] Mudalige T, Qu H, Van Haute D, Ansar SM, Paredes A, Ingle T. Characterization of nanomaterials: Tools and challenges. Nanomaterials for food applications. 2019 Jan 1: 313-53. https://doi.org/10.1016/B978-0-12-814130-4.00011-7.

[23] Gaikwad, V.L., Choudhari, P.B., Bhatia, N.M. and Bhatia, M.S., 2019. Characterization of pharmaceutical nanocarriers: in vitro and in vivo studies. In *Nanomaterials for drug delivery and therapy* (pp. 33-58). William Andrew Publishing. https://doi.org/10.1016/B978-0-12-816505-8.00016-3.

[24] Pate K, Safier P. 12 - Chemical metrology methods for CMP quality. Advances in Chemical Mechanical Planarization (CMP): Elsevier Ltd; 2016. p. 299-325. https://doi.org/10.1016/B978-0-12-821791-7.00017-4.

[25] Joni, I., Zannuary, I., Hidayat, D. and Panatarani, C., 2016, February. A simple microcontroller-based sedimentation potential measurement for nanosuspension stability investigations. In AIP Conference Proceedings (Vol. 1712, No. 1). AIP Publishing. https://doi.org/10.1063/1.4941873.

[26] Rashid TM, Nayef UM, Jabir MS. Nano-ZnO decorated on gold nanoparticles as a core-shell via pulse laser ablation in liquid. Optik (Stuttgart) 2021 Dec; 248: 168164. https://doi.org/10.1016/j.ijleo.2021.168164.

[27] Gannimani R, Ramesh M, Mtambo S, Pillay K, Soliman ME, Govender P. γ-Cyclodextrin capped silver nanoparticles for molecular recognition and enhancement of antibacterial activity of chloramphenicol. Journal of inorganic biochemistry 2016 Apr; 157: 15-24. https://doi.org/10.1016/j.jinorgbio.2016.01.008.

[28] Bélteky P, Rónavári A, Zakupszky D, Boka E, Igaz N, Szerencsés B, et al. Are Smaller Nanoparticles Always Better? Understanding the Biological Effect of Size-Dependent Silver Nanoparticle Aggregation Under Biorelevant Conditions. IJN 2021 -04; Volume16: 3021. https://doi.org/10.2147/IJN.S304138.

[29] Berg JM, Romoser A, Banerjee N, Zebda R, Sayes CM. The relationship between pH and zeta potential of~ 30 nm metal oxide nanoparticle suspensions relevant to in vitro toxicological evaluations. Nanotoxicology. 2009 Dec 1; 3(4): 276-83. https://doi.org/10.3109/17435390903276941.

[30] Seil JT, Webster TJ. Antimicrobial applications of nanotechnology: methods and literature. International journal of nanomedicine. 2012 Jun 6: 2767-81. https://doi.org/10.2147/IJN.S24805.